# Quantitative Estimation of Fe-based Amorphous Coating Thickness Based on Pulsed Eddy Current Technology

**Xiaofei Huang**
Beijing University of Technology
**Zenghua Liu** ( liuzenghua@bjut.edu.cn )
Beijing University of Technology
**Yu Gong**
Beijing University of Technology
**Sha Wu**
Beijing University of Technology
**Kewei Chen**
Beijing University of Technology
**Cunfu He**
Beijing University of Technology

**Research Article**

**Keywords:** PEC, Coating thickness, HVOF, Fe-based amorphous coating, Entropy

**Posted Date:** May 18th, 2022

**DOI:** https://doi.org/10.21203/rs.3.rs-1643989/v1

# Quantitative Estimation of Fe-based Amorphous Coating Thickness Based on Pulsed Eddy Current Technology

Xiaofei Huang, Zenghua Liu, Yu Gong, Sha Wu, Kewei Chen, Cunfu He

*Faculty of Materials and Manufacturing, Beijing University of Technology, Beijing 100124, China*

**Abstract**

Fe-based amorphous coatings prepared by high-velocity oxy-fuel (HVOF) spraying have the advantages of good mechanical properties, high density, low porosity, and high amorphous content. The service life and bonding strength of coating greatly depend on its thickness; however, the characterization of ferromagnetic coating thickness is a very difficult problem. Pulsed eddy current (PEC) is characterized by abundant signals in frequency domains. In this paper, the thickness measurement principle of ferromagnetic coating was explored, and the typical and entropy features from PEC signals were extracted. Seven integrated learning methods were combined to quantitatively characterize the coating thickness, namely Ridge Regression (RR), Lasso Regression (LR), Random Forest Regression (RFR), Extra Trees Regression (ETR), Gradient Boosting Tree Regression (GBTR), Addaptive Boost Regression (ABR) and eXtreme Gradient Boosting Regression (XGBR) algorithms. By comparing typical features with new ones, it was verified that the effective combination of entropy features and typical features could be used as effective feature parameters of eddy current signal. Statistical scores (RMSE and $R^2$) and GridsearchCV features were used to evaluate and optimize the established model. As indicated by the results, the proposed XGBR machine learning model well predicted the coating thickness, and the relative error less than 0.05 mm.

**Keywords:** PEC; Coating thickness; HVOF; Fe-based amorphous coating; Entropy

## 1. Introduction

In Fe-based amorphous coatings have attracted considerable attention in surface engineering owing to their excellent wear and corrosion resistance, high hardness, and excellent bonding strength [1-3]. Hou et al. [4] used a HVOF equipment to deposit Fe-based metallic glass coatings on 316 stainless steel and proved that the coating has superior corrosion resistance in seawater. Peng et al. [5] reported that coating thickness greatly affected the bond strength of the Fe-based amorphous coating prepared by HVOF thermal spraying. Nguyen et al. [6] analyzed the influence of coating thickness on the fatigue life of the Fe-based amorphous coating prepared by HVOF thermal spraying. These findings indicate that coating thickness is a key indicator for evaluating the quality, performance, and service life of Fe-based amorphous coatings. Nondestructive testing is extensively employed for coating thickness measurement; however, commonly used coating thickness measurement and detection techniques have certain limitations. For example, ultrasonic testing requires coupling agents and is not suitable for thin coating thickness measurement, X-ray detection is harmful to human bodies; Terahertz detection technology is suitable for non-conductive coating thickness measurement [7]. However, Fe-based amorphous coatings are ferromagnetic conductive ones. Eddy current testing (ECT) requires no coupling agents and is cheap and suitable for shallow area detection and conductive coating thickness measurement. In comparison to ECT, pulsed eddy current technology (PECT) has the characteristics of abundant signals in frequency domains.

In recent years, PEC has been widely used in coating thickness measurement. Zhang et al. [8] measured the thickness of an anticorrosion coating deposited on a ferromagnetic pipe based on the peak time and the peak value. Wang et al. [9] measured the thickness of a metallic (non-magnetic) coating deposited on a magnetic substrate based on the slope of the lift-off curve on the RL impedance plane. Yao et al. [10] compared the lift-off intersection (LOI) amplitude and time and found that LOI time was better for thickness measurement of non-ferromagnetic coatings on ferromagnetic substrates. Abdelhak et al. [11] adopted the forward modeling model of the coupled electric field method to measure the coating thickness of aviation materials. Cheng et al. [12] measured the thickness of an absorbing coating based on the skin effect. Li et al. [13] quantitatively estimated the thickness and conductivity of non-conductive coating and bond layer of thermal barrier coating. Feature extraction and characterization methods proposed by the above research mainly aim at the thickness measurement of non-conductive coatings and non-magnetic coatings. At present, commercial coating thickness gauges are also mainly used to measure non-ferromagnetic coating thickness on ferromagnetic substrates and non-conductive coating thickness on conductive substrates.

However, Fe-based amorphous coatings have good magnetic conductivity. It is a complex problem to measure the thickness of ferromagnetic coatings. Because the ferromagnetic coating does not meet the requirements of the lift-off effect, it cannot be detected by the conventional ECT. At the same time, the thickness of the substrate is larger than that of coating (on the order of micron), which weakens the penetrating magnetic flux of the loop and hinders the pickup of magnetic signals. Eddy current impedance is affected by complex factors (permeability, conductivity and microstructure), and the received signal contains various information. Therefore, feature extraction is critical to successfully measure the thickness of ferromagnetic coatings.

Generally, entropy function of the uncertain measure in information theory is usually used as the basis of the measure [14, 15]. Shannon et al. [16] proposed the concept of information entropy. Chen et al. [17] adopted information entropy to evaluate the distribution of eddy current sensors. These previous studies indicate that information entropy is likely to be used in eddy current testing (ECT). However, signal amplitude is usually used as a characteristic parameter of coating thickness or defects [18]. The application of information entropy as a characteristic parameter in electromagnetic eddy current nondestructive testing is rarely reported.

In the quantitative estimation of coating thickness, the relationship between coating thickness and features cannot be expressed by a simple mathematical model; thus, it is necessary to introduce a suitable machine learning model to realize thickness inversion. Machine learning is a process of quantization, decision making, and prediction based on a large amount of known data that cannot be solved by traditional mathematical models [19] and has been successfully applied in eddy current detection [20]. Andrea et al. [21] estimated the shape and size of cracks in conductive materials using an artificial neural network (ANN) and a support vector machine based on the principle of eddy current technology. Banerjee et al. [22] proposed a confidence measure based on Bayesian posterior probability to evaluate the confidence of pipe signal classification results in ECT . Vilar et al. [23] extracted 11 specific features based on non-uniformity features for ANN training. Boaretto et al. [24] defined area, eccentricity, and reliability as defect characteristics and trained a feedforward multilayered perceptron.

The machine learning method is effective only if there are reliable input features. In this work, based on typical features, entropy features are proposed as the characteristic parameters of PECT to measure the thickness of Fe-based amorphous coatings. According to the characteristics of the data set, seven machine learning algorithms are used to predict the thickness of the coatings, and entropy features and typical features are compared. The remaining article is structured as follows: In Section 2, the thickness principle of ferromagnetic coating based on magnetic refraction principle is introduced, and the definitions of five entropy features are reviewed. Section 3 briefly describes the preparation process and properties of the coatings and the experimental methods to extract coating thickness signals. In Section 4, seven kinds of machine learning models are established, the accuracy of each model is analyzed, the importance of each entropy feature to the model is determined by calculating the Pearson correlation coefficient, and the accuracies of the model with or without entropy features are compared. Finally, Section 5 draws the main conclusions of this analysis.

## 2. Theory

### *2.1 Thickness measurement principle of ferromagnetic coating*

Magnetic field has the characteristics of aggregation and diffusion. Coating thickness measurement can be explained by the principle of magnetic refraction. When the magnetic induction line is incident from medium 1 (permeability $\mu_1$) to medium 2 (permeability $\mu_2$) at incident Angle $\alpha_1$, magnetic field line is refracted at an Angle $\alpha_2$, as shown in Fig.1. Magnetic field propagation Magnetic field propagation is mainly based on two laws: tangential magnetic field intensity is equal and normal magnetic field intensity is equal

$$\frac{H_1}{B_1}\frac{\sin\alpha_1}{\cos\alpha_1}=\frac{H_2}{B_2}\frac{\sin\alpha_2}{\cos\alpha_2}, \tag{1}$$

where $B_1(H_1)$ and $B_2(H_2)$ is the magnetic induction intensity (magnetic field intensity) of medium 1 and medium 2 respectively.

Because of $B=\mu H$, therefore

$$\alpha_2=\arctan\left(\frac{\mu_1}{\mu_2}\tan\alpha_1\right). \tag{2}$$

According to Eq. (2), it can be concluded that:

(1) When $\mu_1=\mu_2$, $\alpha_1=\alpha_2$, the magnetic pressure at both ends of the interface is consistent, and the magnetic induction line does not deflect.

(2) When $\mu_1\geq\mu_2$, $\alpha_1\geq\alpha_2$, the magnetic field lines are refracted inward in medium 2, almost perpendicular to the interface. The magnetic field diffusion is realized.

(3) When $\mu_1\leq\mu_2$, $\alpha_1\leq\alpha_2$, the magnetic field lines are refracted outwards in medium 2, almost horizontally at the interface. The magnetic field concentration is realized.

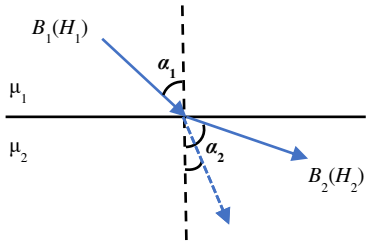


Fig. 1. Magnetic refraction at the interface

It is clear from Eq. (1) that the magnetic declination Angle increases with the increase of permeability. Fig. 2 shows the finite element results of the coating specimen of COMSOL software. When measuring the thickness of ferromagnetic coating such as Fe-based amorphous coating, the air permeability is less than that of ferromagnetic coating, as shown in Figs. 2a). The magnetic field lines generated by the coil refract inside the coating. The magnetic field lines form a closed magnetic circuit with the coil. The signals received by the magnetic sensor are basically all from the coating and are less affected by the substrate. Figs. 2b) shows the distribution of magnetic field lines when the coating is non-ferromagnetic material. It can be seen that no refraction occurs when the magnetic field lines enter the coating, and a large number of magnetic field lines enter the substrate. The ferromagnetic substrate forms a closed magnetic loop with the coil.

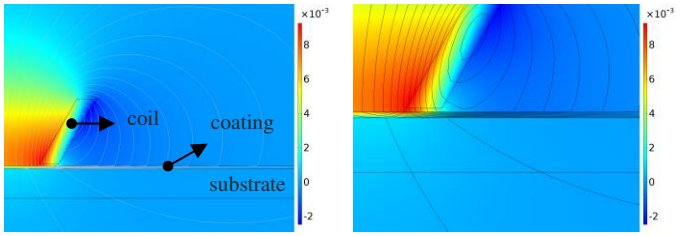


a) Ferromagnetic coating

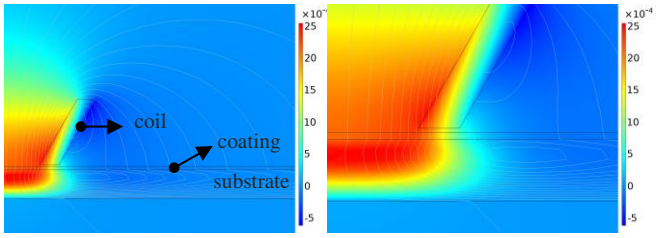


b) Non-ferromagnetic coating

Fig. 2. Magnetic refraction at the interface

*2.2 Entropy*

Entropy is an evaluation standard of information, and it expresses the uncertainty degree of random variables in the form of a numerical value and describes the size of information. The change in the specimen microstructure affect the probability distribution of the waveform. When the magnetic conductivity and electrical conductivity of eddy current propagating in the specimen changes, the disorder of signals increased or decreased, causing a change in the entropy value.

1.Information entropy

Let us assume $X$ is a random variable and its probability is $p(x)$, then the information entropy $H(x)$ can be defined as

$$H(x)=-\sum_{x\in X} p(x)\cdot\log p(x), \tag{3}$$

where the variable $x$ takes all the values in the field. It is clear from Eq. (3) that if the uncertainty of the random variable $x$ is higher, the variable distribution is non-uniform and the information entropy is higher.

2. Conditional entropy

The modified conditional entropy [25] was adopted in this analysis. Let us assume an $N$-dimensional time series $x(1)$, $x(2)$, ..., $x(N)$. The conditional entropy is defined as $CE$, and its calculation process is presented below.

(1) An $L$-dimensional vector is reconstructed from the original time series

$$X_m(i)=\{x(i),x(i+1),...,x(i-L+1)\},\ 1\le i\le N\text{-}L+1. \tag{4}$$

(2) The vector is defined directly by information entropy

$$E(L)=-\sum_{L} p_L\log p_L, \tag{5}$$

where $p_L$ is the joint probability density of the sequence $x$.

(3) Conditional entropy is derived directly from the difference of information entropy

$$CE=E(L)-E(L-1). \tag{6}$$

3 Sample entropy

The sample entropy ($SampEn$) of the $N$-dimensional time series $x(1)$, $x(2)$, ..., $x(N)$ is defined according to the method proposed in the literature [26].

(1) An $m$-dimensional vector is constructed from the original time series

$$X_m(i)=\{x(i),x(i+1),...,x(i+m-1)\},\ 1\le i\le N\text{-}m+1. \tag{7}$$

(2) The distance between $X_m(i)$ and $X_m(j)$ is defines as

$$d[Xm(i),Xm(j)]=\max_{k\in[1,m-1]}\left(\left|x(i+k)-x(j+k)\right|\right). \tag{8}$$

(3) Let assume tolerance is $r$. The number of $d[Xm(i),Xm(j)]\leqslant r$ corresponding to each $X_m(i)$ is counted and denoted as $A_i$. The ratio of $A_i$ to $N-m+1$ is defined as

$$B_i^m(r)=\frac{A_i}{N-m+1},1\le i\le N-m. \tag{9}$$

(4) The average value ( $B^m(r)$ ) of $B_i^m(r)$ is calculated as

$$B^m(r)=\frac{1}{N-m}\sum_{i=1}^{N-m}B_i^m(r), \tag{10}$$

(5) The value of $B^{m+1}(r)$ is obtained by the same method. When $N$ is finite, $SampEn$ is

$$SampEn(m,r)=-\ln\frac{B^{m+1}(r)}{B^m(r)}, \tag{11}$$

where the similarity tolerance $r$ ranged from 0.1 to 0.3SD (SD is the standard deviation of the time series). In this calculation, $r$ is 0.1SD and point $N$ is the signal length. $M$ adopted the false nearest neighbor point (FNN) algorithm to estimate the embedding dimension of phase space reconstruction.

4. Fuzzy entropy

The fuzzy entropy ($FuzzyEn$) of the $N$-dimensional time series $x(1)$, $x(2)$, ..., $x(N)$ is defined according to the method proposed in the literature [27].

(1) The original time series constituted an $m$-dimensional vector minus its mean value

$$X_m(i)=\{x(i),x(i+1),...,x(i+m-1)\}-x_0(i), \tag{12}$$

where $x_0(i)$ is the average of $x(i)$.

(2) The distance between $X_m(i)$ and $X_m(j)$ is defined as

$$d[Xm(i),Xm(j)]=\max_{k\in[1,m-1]}\left(\left|\left|x(i+k)-x_0(i)\right|-\left|x(j+k)-x_0(j)\right|\right|\right). \tag{13}$$

(3) The similarity of the exponential membership function calculation mode is introduced

$$A(x)=\exp\left(-\ln\left(\frac{x}{r}\right)^2\right). \tag{14}$$

(4) The average of $A_{ij}$ is introduced

$$\varphi^m(r)=(N-m+1)^{-1}\sum_{i=1}^{N-m+1}C_i^m(r), \tag{15}$$

where $\varphi^{m+1}(r)$ is obtained by the same method. When $N$ is finite, fuzzy entropy could be defined as

$$FuzzyEn(m,r)=-\ln\frac{\varphi^{m+1}(r)}{\varphi^m(r)}. \tag{16}$$

5 KL divergence

KL divergence (Kullback-Leible divergence) is also known as relative entropy, and it measured the similarity of two probability density distribution functions in information theory. The smaller the KL value of two probability density distribution functions, the smaller the difference of the two functions [28]. Let us assume $p(x)$ and $q(x)$ are two discrete probability distribution functions, and their divergence values are

$$D_{KL}\left(p\|q\right)=\sum_{i=1}^{n}p\left(x\right)\log\frac{p\left(x\right)}{q\left(x\right)}. \tag{17}$$

KL divergence has asymmetric characteristics and reflects the distance between two probability density distribution functions; however, it does not consider that the distance is symmetric. KL divergence can be proved to be non-negative by Gibbs inequality. To meet the above two characteristics of KL divergence, KL divergence is redefined as

$$KL=D_{KL}\left(p\|q\right)+D_{KL}\left(q\|p\right). \tag{18}$$

In this analysis, $p(x)$ and $q(x)$ are represented by coated and uncoated signals, respectively.

## 3. Material and method

### *3.1 Material preparation and properties*

The investigated Fe-based amorphous coating was prepared on a 316 stainless steel substrate of 150 mm (H) × 80 mm (W) × 5 mm (D) by HVOF. The Fe-based amorphous powder was mainly composed of Fe, Cr, and Ni (Table 1).

**TABLE 1**
Chemical composition of Fe-based powder

| Chemical element | Fe | Cr | Ni |
|---|---|---|---|
| Content (%) | 74.02 | 17.46 | 2.74 |

In the Praxair JP5000 HVOF spraying system, jet kerosene and oxygen were used as the fuel and accelerant, respectively. The spraying powder was transported by a powder feeder, and the powder was sent to the flame through radial powder feeding. Nitrogen was used as the carrier gas for powder feeding. The pressure in the combustion chamber was 6.7 MPa, the flow rate of kerosene was 5.8 L/h, and the feeding rate was 4.5 g/min. Before spraying, the matrix surface was coarsened by 30 mesh brown corundum and then ultrasonically cleaned with alcohol.

The XRD pattern of the Fe-based amorphous coating was detected by an Haoyuan DX2700-BH diffractometer (Fig. 3). A diffuse scattering diffraction peak appeared at $2\theta$ = 45°, indicating the formation of an amorphous structure during the spraying process. The morphology of the coating is displayed in Fig. 4. The surface roughness (*R*a) of the coating was measured as 4.8 by a JITAI KEYI surface roughness tester.

The coating thickness was calibrated by measuring the thickness difference before and after spraying with a micrometer. However, an unavoidable thickness calibration error occurred due to different roughness values and bonding strengths before and after spraying, and the error was lower than 20 μm.

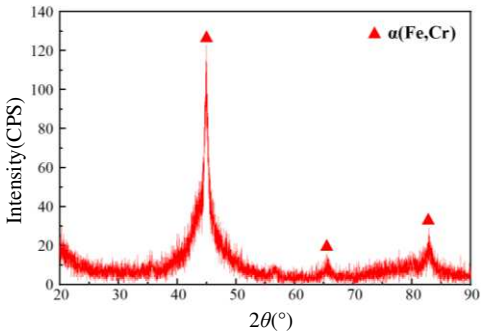

Fig. 3. XRD pattern of the Fe-based amorphous coating

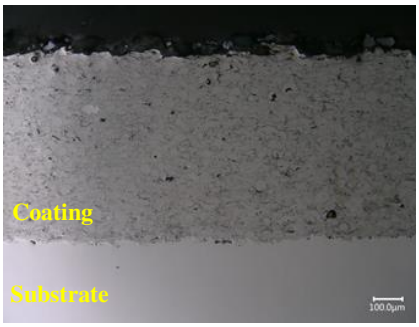

Fig. 4. Morphology of the Fe-based amorphous coating

### *3.2 Experimental System*

The experimental platform of PEC is displayed in Fig. 5. The platform included an oscilloscope (MDO4054C), a function generator (AFG3021B), a DC power supply (KA3005P), and a cone-shaped PEC probe. The Fe-based amorphous coating was a magnetic conductive one and thin. Generally, any change in coating thickness greatly affects magnetic field signals; thus, the magnetic probe was used. To improve the magnetic gathering ability, an iron core and a magnetic shield were added to the center of the probe. However, magnetization inevitably occurs in ferromagnetic coatings. Compared with the traditional PEC probe, this cone-shaped PEC probe could concentrate the magnetic field and be also sensitive to the change of weak signals [29]. The function generator excited square wave signals with an amplitude of 10 V, a frequency of 5 kHz, and a duty cycle of 50%. The DC power supply was used to supply power to the Hall probe, and the oscilloscope was used to collect and display signals.

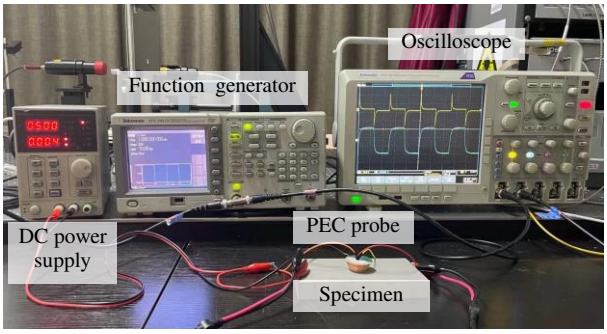

Fig. 5. Schematic diagram of PECT experimental system

Signals received from Fe-based amorphous coating samples with different thicknesses (0.1-0.5 mm, thickness difference = 0.1 mm) by the Hall probe are exhibited in Fig. 6.

It is noticeable that the signal amplitude increased gradually with the increase of the coating thickness. However, the larger the coating thickness, the smaller the amplitude change, indicating that the amplitude change was affected by the skin effect of eddy current. Fig. 7 present the normalized amplitude of typical features, including amplitude (Vpp) and fundamental wave amplitude (Vpp_fd). Fig. 8 show the normalized amplitude of entropy features extracted according to Eqs. (2)-(18). KL divergence, information entropy, and fuzzy entropy increased or decreased with thickness, sample entropy, and conditional entropy changed irregularly. It is evident that both typical characteristic and non-characteristic parameters were nonlinear. If a mathematical model is used to express them, thickness inversion cannot be achieved; therefore, it is necessary to introduce machine learning model training.

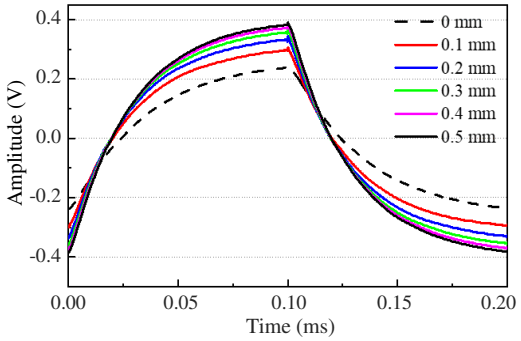


Fig. 6. Received waveforms of PECT probe.

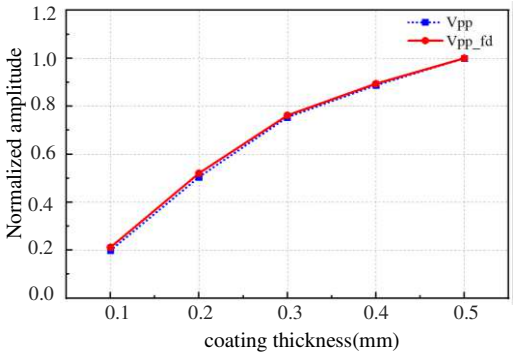


Fig. 7. Normalized amplitude of typical characteristic parameters

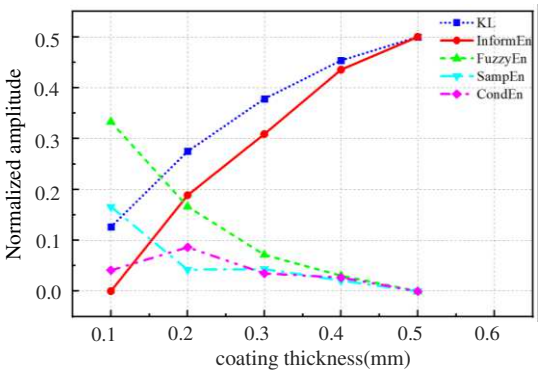


Fig. 8. Normalized amplitude of entropy characteristic parameters

## 4. Machine learning algorithms

### *4.1 RR algorithm model*

RR model is an improvement on the least square method, which regularizes the linear model by changing the weight of the model [30]. The Ridge algorithm essentially adds $L_2$ regular term to the loss function of linear regression, and its cost function is as follows

$$J(\theta) = MSE(\theta) + \alpha \frac{1}{2} \sum_{i=1}^{n} \theta^2 , \tag{19}$$

where $J(\theta)$ is the cost function, $\alpha$ is the hyperparameter, $\theta$ is the offset term.

The RR equation has a slightly lower coefficient of determination than the conventional regression model, but it has a higher significance. It has a good prediction effect for data sets with collinearity and ill-condition.

### *4.2 LR algorithm model*

LR model is also regularized by changing the weight of the linear model and adding weight to the $L_1$ regular term. LR model does not penalize the parameters of the model twice, but instead penalizes the compressed regression coefficients twice. Therefore, the cost function of improving the ill multicollinearity of the model is as follows[31]

$$J(\theta) = MSE(\theta) + \alpha \sum_{i=1}^{n} |\theta_i| , \tag{20}$$

Since LR model uses $L_1$ regular term, which reduces the useless feature coefficients of the result and highlights the useful feature coefficients of the result. LR algorithm has feature selection ability.

### *4.3 RFR algorithm model*

RFR algorithm is a ensemble learning method based on a large number of decision trees, which is an extension of Bagging method. The RFR partitions the data set using multiple put-back sampling technique. The sampling process is to extract $N$ training sets from the original data set, and each training set is about two-thirds of the size of the original data set. A total of $N$ decision trees are constructed to form a random forest. In the growth process of each tree, each node is segmented with some randomly selected attributes. The final regression decision calculation formula is as follows

$$H(x) = \frac{1}{K} \sum_{i=1}^{K} t_i(x) \tag{21}$$

where $t_i(x)$is the regression model sequence, $K$ is the mount of decision trees.

The prediction result of RFR model is relatively stable on unbalanced data sets, which can deal with high-dimensional data and improve the prediction accuracy while keeping the computation constant. However, the model is prone to over-fitting in the case of high noise[32].

### *4.4 ETR algorithm model*

ETR is a machine learning algorithm model combining ensemble learning and random forest theory. How to divide decision tree nodes is the main difference between ETR and RFR models. When dividing nodes, ETR model randomly selects eigenvalues instead of searching and comparing. Such node division provides additional randomness to the model, which improves the training speed and over-fitting behavior of the model, but also increases the possibility of model decision deviation. ETR can process high-dimensional data and achieve high accuracy prediction, so it is widely used in image processing, artificial intelligence, information recognition and other fields[33].

*4.5 GBTR algorithm model*

GBTR is a decision tree method, which is an improvement of Boosting algorithm. The core idea of GBTR is to combine several weak learners in series to form a strong learner. In GBTR training, loss function is used to reduce residual and generate a new decision tree. GBTR algorithm has good processing effect in both continuous and discrete values, and the accuracy will be improved when appropriate parameters need to be set in the model. However, due to the interdependence of weak learners in the model, training data cannot be processed in parallel, so good training effects cannot be achieved for data with high-dimensional sparse features[34].

GBTR outputs prediction results in parallel, and each weak learner is the negative gradient of the loss function of the previous weak learner, which can improve the accuracy of prediction. Compared with the traditional decision tree and RF model, the variance and bias of this model are improved.

*4.6 ABR algorithm model*

ABR model can automatically adjust the weight according to the estimation error. The core idea of ABR model is to obtain multiple weak learners through continuous iteration, and finally combine them into one strong learner. ABR obtains the weight parameter $\alpha_t$ of the weak learner by taking a minimum of the exponential loss function. However, this model is sensitive to discrete points and is prone to noise interference. In the iterative process, abnormal samples tend to get a high weight, thus affecting the accuracy of the final prediction results.

ABR algorithm has high speed, few adjustable parameters and no high requirements for weak learners. Since the ABR algorithm changes the weight of the sample iteratively, it can correct the samples that are not correctly learned[35].

*4.7 XGBR algorithm model*

The thickness of a coating is related to many factors. Numerous known and unknown factors influence the appearance of pores and cracks in a coating during the preparation process and consequently, affect eddy current signals. XGBR, a machine learning method, was used to determine the relationship between output and input data. It is an improved algorithm for traditional gradient boost. XGBR used the second derivative function approximation for the objective function and introduced regular terms into the objective function to obtain the optimal solution. The objective function of XGBR consisted of its own loss function and regularization term, which could effectively reduce the over-fitting problem and improve the algorithm efficiency [19]. In comparison to other machine learning algorithms, this model has the advantages of fast operation speed and strong generalization ability.

$$O_{bj} = \sum_{i=1}^{n} l\left(y_i, \hat{y}_i\right) + \sum_{k=1}^{K} \Omega\left(f_i\right), \tag{22}$$

where $\sum_{i=1}^{n} l\left(y_i, \hat{y}_i^t\right)$ is the loss function that indicates the deviation between the predicted value and the real value, $t$ is the number of iterations, $\Omega\left(f_i\right)$ is a regular term that represents the complexity of the tree model, and $K$ is the number of regression trees.

## 5. Quantitative analysis

*5.1 Data collection and standardization*

Signals collected from ten coating samples (0.1-0.5 mm) were extracted, and each specimen was randomly sampled 20 times. Typical features (peak value and fundamental wave amplitude in the frequency domain) and entropy features (KL divergence, information entropy, fuzzy entropy, sample entropy, conditional entropy) were extracted. As different characteristic values vary in amplitude, the collected data were normalized and scaled to the range of [0, 1].

$$x' = \frac{x_i - \min\left(x\right)}{\max\left(x\right) - \min\left(x\right)}, \tag{23}$$

where $x_i$ is the characteristic parameter, and min($x$) and max($x$) are the minimum and maximum values of the characteristic parameter, respectively.

*5.2 Feature selection*

Under the condition of large samples, the Pearson correlation coefficient analysis was conducted among typical features, new features, and coating thickness (Fig. 9). It is clear that typical features, information entropy, fuzzy entropy, sample entropy, and KL divergence all have a positive and negative correlation, and it is consistent with the variation rule shown in Figs. 7 and 8. However, the conditional entropy correlation coefficient was low; hence, this feature was removed.

In the learning process, the data set has 200 sets of signals: 70% of them were used for training and the rest for testing. Typical features, entropy features, and vectors composed of typical and entropy features were employed to train the model, and the RMSE and $R^2$ of the model are presented in Table 2.

**Table 2**
Vector input result

| Combination of features | $R^2$ | RMSE |
|---|---|---|
| Typical features | 0.997783 | $4.68 \times 10^{-5}$ |
| Entropy features | 0.999063 | $1.97 \times 10^{-5}$ |
| Combination of typical and entropy features | 0.999232 | $1.62 \times 10^{-5}$ |

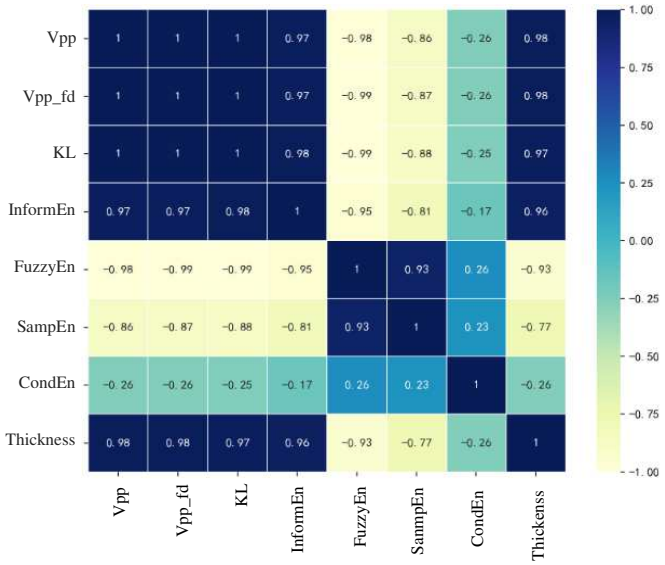


Fig. 9. Pearson correlation coefficient

As can be seen from the Table 2, when entropy features were used as inputs, RMSE and $R^2$ were both larger than those with typical features. The combination of typical and entropy features led to better results in comparison to either one alone. These three entropy features were found to be more accurate in quantifying coating thickness than typical features. By combining typical features with entropy features, the deficiency of single feature parameters was compensated.

*5.4 Hyperparameter optimization*

To obtain the best prediction performance for the collected data set, Gridsearch-CV technology was used to optimize the main hyperparameters of the seven models under the optimal feature combination. Each group of hyper-parameters was evaluated by cross-validation method. The optimal parameters of the optimal prediction performance are presented in Table 3.

**Table 3**
Optimal hyperparameters obtained by Gridsearch-CV

| Machine learning model | Parameter Name | Parameter setting |
|---|---|---|
| XGBR | n_estimators | 60 |
| | learning_rate | 0.2 |
| | max_depth | 3 |
| GBTR | n_estimators | 100 |
| | learning_rate | 0.1 |
| | max_depth | 3 |
| | subsample | 0.7 |
| RFR | n_estimators | 75 |
| | max_depth | 10 |
| ETR | random_state | 10 |
| | max_depth | 3 |
| ABR | n_estimators | 20 |
| | learning_rate | 0.5 |
| RR | alphas | 0.001 |
| LR | Eps | 0.0001 |
| | n_alphas | 100 |

*5.5 Model analysis*

The coating thickness was taken as the output parameter, and the six eigenvalues of the combination of the entropy feature parameters and the typical feature parameters were used as the input parameters to train the seven regression models including XGBR, GBTR, RF, ETR, ABR, RR and LR. As shown in Fig. 10, the scatter diagram of model prediction is added with 95% confidence curve. When the data falls on the diagonal, the prediction result is highly correlated with the real value. It is worth noting that when the prediction results are more accurate, the data are relatively concentrated.

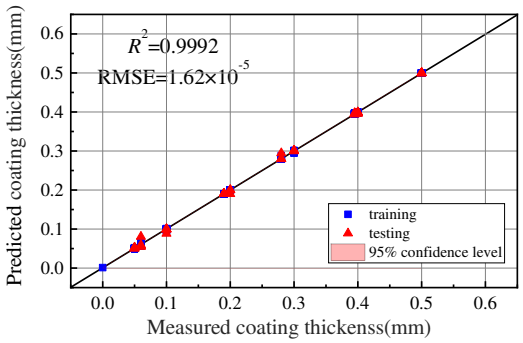


a) XGBR predicted results

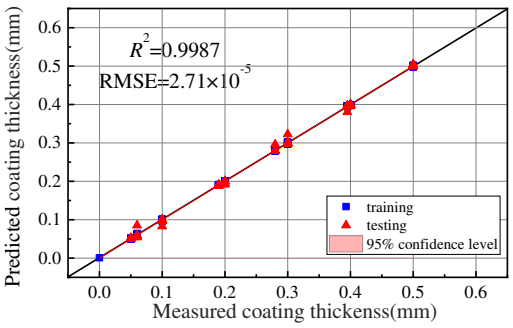


b) GBTR predicted results

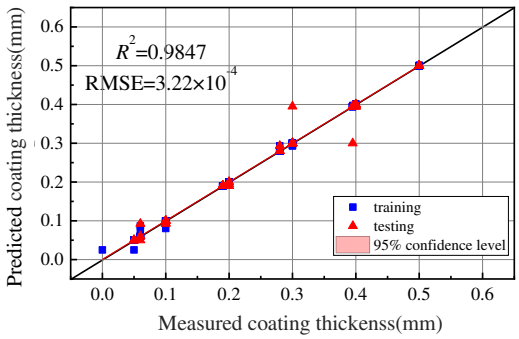


c) RFR predicted results

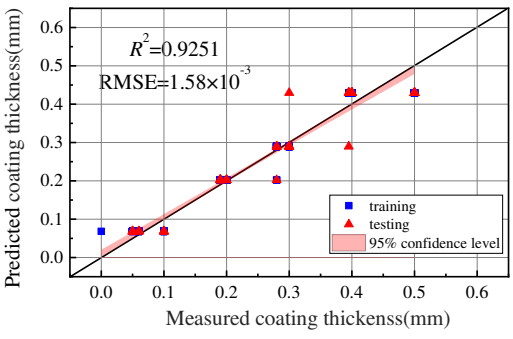


d) ETR predicted results

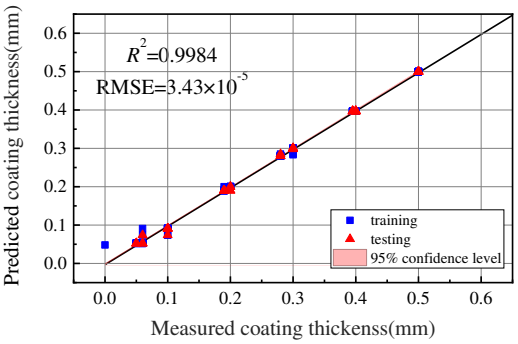


e) ABR predicted results

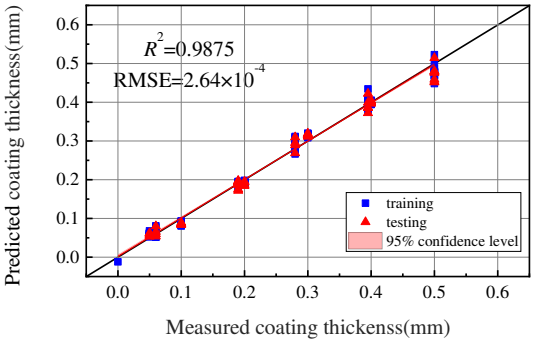


f) RR predicted results

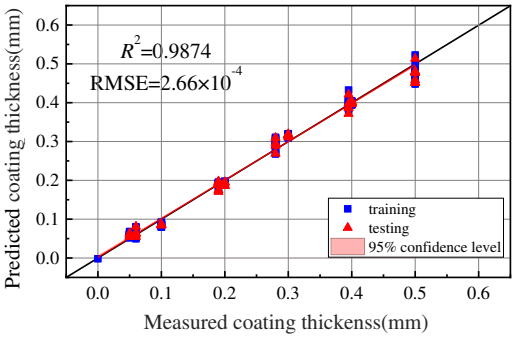


g) Lasso predicted results

Fig. 10. Predicted vs measured.

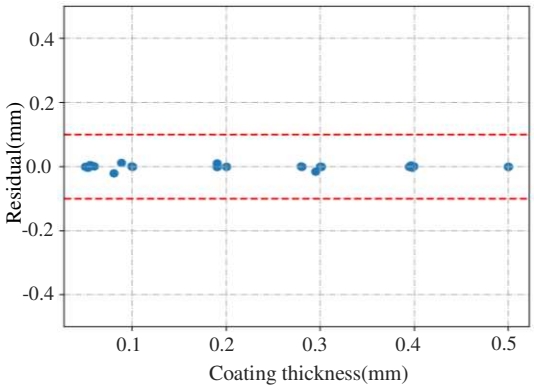


Fig. 11. Plot of residuals.

As can be seen from the Fig. 11, the training effect of most models is good, and the data points are basically distributed near the diagonal. XGBR model had the best prediction ability ($R^2$=0.9992, RMSE=1.62×10$^{-4}$), followed by GBTR model ($R^2$=0.9988, RMSE=2.54×10$^{-4}$), and ETR model ($R^2$=0.9251, RMSE = 1.58×10$^{-4}$).

It is noticeable from Fig. 11 that the size of residuals was less than 0.05 mm. It shows that XGBR model has great advantages in thickness measurement of Fe-based amorphous coatings.

## 6. Discussion

Fe-based amorphous coatings are ferromagnetic ones. The excitation source generated current and induced a magnetic field in the coating. According to the magnetic refraction theory, most of the incoming magnetic circuit passes through the coating and the excitation source to form a closed magnetic circuit, and the coating thickness directly affected the size of the induced magnetic field and the received signal. The cone-shaped probe, which played a significant role in gathering the magnetic field, was combined with entropy features to improve

its detection accuracy.

Entropy features successfully characterized the coating thickness, because the changes in the permeability, conductivity, microstructure, and thickness of the coating led to an increase or decrease of signal disorder and consequently changed the entropy value. As the coating thickness increased, the amount of information contained in the received signal increased; thus, the information entropy increased. KL divergence was used to represent the difference between two probability density distributions. The higher the difference between two probability density distributions, the greater the KL divergence. In this paper, the two probability distributions represent the signal with or without coating. As the thickness of the coating increases, so does their difference. Fuzzy entropy is the optimization of sample entropy. By introducing fuzzy function, the result is more accurate.

The XGBR has better prediction effect compared with seven machine learning models. Since the sample size of this experiment is relatively sparse, and XGBR has a good effect in processing sparse samples. Therefore, this model is suitable for predicting the thickness of Fe-based amorphous coating.

## 6. Conclusions

This paper proposed the quantitative estimation of ferromagnetic coating thickness based on PEC and explored the measurement mechanism of ferromagnetic coating thickness. A novel signal extraction method based on entropy features was proposed to analyze the change of coating thickness. The Pearson correlation algorithm of machine learning was used to select feature parameters relating to coating thickness characteristics. The results show that the goodness of fit for the combination of entropy features and typical features was more accurate than that with typical features. Then the hyperparameters of the seven machine learning model were optimized. After comparison of model evaluation indexes, XGBR machine learning model can predict the result well ($R^2$=0.9992, RMSE=$1.62\times10^{-4}$).

The proposed quantitative estimation method had higher goodness of fit. Entropy features proposed in this work could be applied not only to coating thickness measurement, but also to other eddy current testing fields such as defect detection.

Further research can be carried out:(1) Due to cost and time constraints, the sample data volume can be increased in the future; (2) Scanning electron microscope can be used to mark the sample data and to improve the detection accuracy; (3) Further explore the relationship between eddy current signal and entropy characteristics.

**Ethics approval and consent to participate** Not applicable.
**Consent for publication** Published informed consent were obtained from all participants.
**Availability of data and material** Not applicable.
**Competing interests** The authors have declared that no competing interests exist.
**Funding** Not applicable.

**Authors' contributions** Xiaofei Huang and Zenghua Liu wrote the main manuscript text. Sha Wu prepared figure 5. Kewei Chen prepared figures 3-4. Yu Gong and Cunfu He participated in the discussion. All authors reviewed the manuscript.
**Authors' information** Not applicable.
**Acknowledgements** This study was supported in part by the National Key Research and Development Program of China under Grant 2018YFC1902404, in part by the National Natural Science Foundation of China under Grant 11772014.

## References

[1] Weiyan Lu, Debin Wang, Qi Wang, et al, Sensitivity of corrosion behavior for Fe-based amorphous coating to temperature and chloride concentration, Coatings 11(3) (2021) 331.
[2] S. Vignesh, K. Shanmugam, V. Balasubramanian, K. Sridhar, D. Thirumalaikumarasamy, et al, Electrochemical corrosion behaviour of HVOF sprayed iron-based amorphous metallic coatings on AISI 316 stainless steel in an NaCl solution, Journal of the Mechanical Behavior of Materials 27(3-4) (2018) 20180015.
[3] Yasir Muhammad, Zhang Cheng, Wang Wei, et al, Tribocorrosion behavior of Fe-Based amorphous composite coating reinforced by Al2O3 in 3.5% NaCl Solution, Joural of Thermal Spray Technology 25(8) (2016) 1-7.
[4] Guoliang Hou, Xiaoqin Zhao, Huidi Zhou, et al, Cavitation erosion of several oxy-fuel sprayed coatings tested in deionized water and artificial seawater, Wear 311(1-2) (2014) 81-92.
[5] Y. Peng, C. Zhang, L. Liu, et al, On the bonding strength in thermally sprayed Fe-based amorphous coatings, Surface & Coatings Technology, 218 (2013) 17-22.
[6] Vinh Phoi Nguyen, Thien Ngon Dang, Chi Cuong Le, et al, Effect of coating thickness on fatigue behavior of AISI 1045 steel with HVOF thermal spray and hard chrome electroplating, Journal of Thermal Spray Technology 29(8) (2020) 1968-1981.
[7] Shrestha Ranjit, Yoonjae Chung, Wontae Kim, Thermal behavior variations in coating thickness using pulse phase thermography, Journal of the Korean Society for Nondestructive Testing 36(4) (2016) 259-265.
[8] Jianhai Zhang, Maodan Yuan, Sung-Jin Song, et al, Precision measurement of coating thickness on ferromagnetic tube using pulsed eddy current technique, International Journal of Precision Engineering and Manufacturing 16(8) (2015) 1723-1728.
[9] Hongbo Wang, Wei Li, Zhihua Feng, Noncontact thickness measurement of metal films using eddy-current probes immune to distance variation, IEEE Transactions on Instrumentation and Measurement 64(9) (2014) 1-1.
[10] Yao Wang, Mengbao Fan, Binghua Cao, et al, Measurement of coating thickness using lift-off point of intersection features from pulsed eddy current signals, NDT and E International 116 (2020) 102333.
[11] Abdelhak Abdou, Tarik Bouchala1, Bachir Abdelhadi, et al, Nondestructive eddy current measurement of coating thickness of aeronautical construction materials, Instrumentation Mesure Métrologie. 18(5) (2019) 451-457.
[12] Yuhua Cheng, Yifan Chen, Jixiang Jiang, et al, Absorbing coating thickness measurement based on lift-off effect of eddy current testing. International Journal of Applied Electromagnetics and Mechanics 45(1-4) (2014) 323-330.
[13] Yong Li, Zhenmao Chen, Ying Mao, et al, Quantitative evaluation of thermal barrier coating based on eddy current technique, NDT and E International 50 (2012) 29-35.
[14] J.N. Kapur, P.K. Sahoo, A.K.C. Wong, A new method for gray-level picture thresholding using the entropy of the histogram, Computer Vision, Graphics, and Image Processing 29 (1985) 273-285.
[15] S.M. Hosseini, A. Ghasemi-Ghalebahman, M. Azadi, et al, Crack initiation detection in crankshaft ductile cast iron based on information entropy of acoustic emission signals under tensile loading, Engineering Failure Analysis 127 (2021) 105547.
[16] C E Shannon. A mathematical theory of communication. ACM SIGMOBILE mobile computing and communications review, 2001, 5(1): 3-55.
[17] G. Chen, Z. Cao, Quantitative evaluation of eddy current distribution by relative entropy and cross entropy, Measurement and Control 54(3-4)

(2021) 164-169.
[18] Zenghua Liu, Jiufu Yao, Cunfu He, et al, Development of a bidirectional-excitation eddy-current probe with magnetic shielding: Detection of subsurface defects in stainless steel, IEEE Sensors Journal 18(15) (2018) 6203-6216.
[19] Chaoliang Xu, Xiangbing Liu, Hongke Wang, et al, A study of predicting irradiation-induced transition temperature shift for RPV steels with XGBoost modeling, Nuclear Engineering and Technology 53(8) (2021) 2610-2615.
[20] Jan Behmann, Anne Katrin Mahlein, Till Rumpf, et al, A review of advanced machine learning methods for the detection of biotic stress in precision crop protection. Precision Agriculture 16(3) (2015) 239-260.
[21] Andrea Bernieri, Luigi Ferrigno, Marco Laracca, et al, Crack shape reconstruction in eddy current testing using machine learning systems for regression. IEEE Transactions on Instrumentation and Measurement 57(9) (2018) 1958-1968.
[22] Portia Banerjee, Lalita Udpa, Satish Udpa, et al, Confidence metric for signal classification in non destructive evaluation, NDT and E Int 91 (2017) 88-96.
[23] Rafael Vilar, Juan Zapata, Ramo´n Ruiz, An automatic system of classification of weld defects in radiographic images, NDT and E Int 42(5) (2009) 467-476.
[24] Neury Boaretto, Tania Mezzadri Centeno, Automated detection of welding defects in pipelines from radiographic images DWDI, NDT and E Int 86 (2017) 7-13.
[25] A. Porta, G. Baselli, D. Liberati, et al, Measuring regularity by means of a corrected conditional entropy in sympathetic outflow, Biological Cybernetics 78(1) (1998) 71-78.
[26] Richman J S, Moorman J R, Physiological time-series analysis using approximate entropy and sample entropy. American Journal of Physiology-Heart and Circulatory Physiology 278(6) (2000) H2039-H2049.
[27] Weiting Chen, Zhizhong Wang, Hongbo Xie, et al, Characterization of surface EMG signal based on fuzzy entropy, IEEE Transactions on neural systems and rehabilitation engineering 15(2) (2007) 266-272.
[28] Wahiba Bounoua, Amina B. Benkara, Abdelmalek Kouadri, et al, Online monitoring scheme using principal component analysis through Kullback-Leibler divergence analysis technique for fault detection. Transactions of the Institute of Measurement and Control 42(6) (2020) 1225-1238.
[29] Yu Gong, Xiaofei Huang, Zenghua Liu, et al, Development of a cone-shaped pulsed eddy current probe, IEEE Sensors Journal, 22(4) (2022) 3129-3136.
[30] Xiuhua Li, Lin Ma, Xuezhi Tan, Xin Liu, Novel Pilot-aided Ridge Regression Channel Estimation for SC-FDE System on Time-varying Frequency Selective Fading Channel.Journal of Harbin Institute of Technology 20(1) (2013) 23-27.
[31] Michael Döhler, Qinghua Zhang, Laurent Mevel, Damage localization in mechanical systems by Lasso regression, IFAC-PapersOnLine 54(7) (2021) 286-29
[32] Runhong Zhang, Yongqin Li, Anthony T.C.Goh, Analysis of ground surface settlement in anisotropic clays using extreme gradient boosting and random forest regression models, Journal of Rock Mechanics and Geotechnical Engineering 13(6) (2021) 1478-1484.
[33] Vinod Nistane, Suraj Harsha, et al, Performance evaluation of bearing degradation based on stationary wavelet decomposition and Extra Trees Regression, World Journal of Engineering (2018) 00-00.
[34] FangfangYang, DongWang, FanXu, et al, Lifespan prediction of lithium-ion batteries based on various extracted features and gradient boosting regression tree model, Journal of Power Sources 476 (2020) 228654.
[35] S.B. Koduri, L. Gunisetti, C.R. Ramesh, K.V. Mutyalu, et al, Prediction of crop production using adaboost regression method, Journal of Physics Conference Series 1228 (2019) 012005.